Atmos. Chem. Phys. Discuss., 15, 17229–17250, 2015
www.atmos-chem-phys-discuss.net/15/17229/2015/
doi:10.5194/acpd-15-17229-2015
© Author(s) 2015. CC Attribution 3.0 License.

Atmospheric Chemistry and Physics Discussions
Open Access

This discussion paper is/has been under review for the journal Atmospheric Chemistry and Physics (ACP). Please refer to the corresponding final paper in ACP if available.

How large-scale subsidence affects stratocumulus transitions

J. J. van der Dussen[1], S. R. de Roode[1], and A. P. Siebesma[2,1]

[1]Department of Geoscience and Remote Sensing, Delft University of Technology, Delft, the Netherlands
[2]Royal Netherlands Meteorological Institute (KNMI), De Bilt, the Netherlands

Received: 18 May 2015 – Accepted: 27 May 2015 – Published: 24 June 2015

Correspondence to: J. van der Dussen (johanvanderdussen@outlook.com)

Published by Copernicus Publications on behalf of the European Geosciences Union.

How large-scale subsidence affects stratocumulus transitions

van der Dussen et al.

Abstract

Some climate modeling results suggest that the Hadley circulation might weaken in a future climate, causing a subsequent reduction in the large-scale subsidence velocity in the subtropics. In this study we analyze the cloud liquid water path (LWP) budget from large-eddy simulation (LES) results of three idealized stratocumulus transition cases each with a different subsidence rate. As shown in previous studies a reduced subsidence is found to lead to a deeper stratocumulus-topped boundary layer, an enhanced cloud-top entrainment rate and a delay in the transition of stratocumulus clouds into shallow cumulus clouds during its equatorwards advection by the prevailing trade winds. The effect of a reduction of the subsidence rate can be summarized as follows. The initial deepening of the stratocumulus layer is partly counteracted by an enhanced absorption of solar radiation. After some hours the deepening of the boundary layer is accelerated by an enhancement of the entrainment rate. Because this is accompanied by a change in the cloud-base turbulent fluxes of moisture and heat, the net change in the LWP due to changes in the turbulent flux profiles is negligibly small.

1 Introduction

As subtropical marine stratocumulus clouds are advected by the tradewinds over increasingly warm water they are often observed to transition into shallow cumulus clouds. Such transitions involve a rapid decrease of the cloud cover and the cooling effect due to the presence of low clouds is hence diminished. Therefore, a change of the pace of stratocumulus transitions in a future climate could potentially be of importance for the magnitude of the cloud-climate feedback.

Some general circulation model results suggest that the Hadley-Walker cell may weaken as a result of climate warming (e.g. Held and Soden, 2006; Vecchi and Soden, 2007). In the subtropical part of the Hadley cell there is a mean subsiding motion of air. It is therefore reasonable to assume that the large-scale subsidence in subtropical ar-

ACPD
15, 17229–17250, 2015

CC BY

eas will weaken in a future climate. A weakening of the large-scale subsidence caused an increase of the liquid water path (LWP) of stratocumulus layers within a steady-state Eulerian framework (Blossey et al., 2013; Bretherton et al., 2013). As such, reduced subsidence might be one of the few processes to cause additional cloudiness in a future climate scenario (Bretherton and Blossey, 2014). It is therefore of paramount importance to have a thorough understanding of how a weakening of the large-scale subsidence increases the LWP and the life-time of stratocumulus clouds.

Together with the entrainment rate, the subsidence velocity determines the rate of deepening of boundary layers that are capped by an inversion, as follows

$$\frac{dz_i}{dt} = w_e + \overline{w}(z_i). \tag{1}$$

Here, z_i is the height of the inversion, t is time, w_e is the entrainment velocity and $\overline{w}$ is the large-scale subsidence velocity. A lower subsidence velocity therefore leads to a more rapid deepening of the boundary layer if the entrainment velocity remains unaffected. Such deeper boundary layers are often assumed to be less well mixed than shallow boundary layers (Park et al., 2004; Wood and Bretherton, 2004). It was therefore hypothesized that weaker subsidence could increase the pace of stratocumulus transitions (e.g. Wyant et al., 1997; Bretherton et al., 1999).

Svensson et al. (2000), however, used a one-dimensional turbulence model to show that the moment of break up of the stratocumulus layer is actually delayed when the magnitude of the large-scale subsidence velocity is decreased. Later, Sandu and Stevens (2011) corroborated these findings by performing several large-eddy simulations (LESs) of stratocumulus transition cases. Moreover, Myers and Norris (2013) found from observations that low cloud amount in the subtropics tends to decrease as subsidence becomes stronger.

This study investigates the effect of a change in the strength of the Hadley circulation, as quantified by the large-scale subsidence velocity, on the typical time scale of the break up of stratocumulus and its subsequent transition to broken shallow cumulus.

ACPD
15, 17229–17250, 2015

CC BY

The entrainment rate as well as the subsidence velocity are typically poorly constrained by observations (Bretherton et al., 1995; De Roode and Duynkerke, 1997; Ciesielski et al., 2001; Carman et al., 2012) or by reanalysis products (Duynkerke et al., 1999). For this reason, LES is used here. A budget equation for the tendency of the LWP of the stratocumulus layer as derived by Van der Dussen et al. (2014) is used to analyze the LES results in order to determine the role of each individual physical processes during stratocumulus transitions. Through this analysis, insight is gained into how subsidence affects the pace of stratocumulus transitions, which helps to determine the robustness of the sign of the response to a weakening subsidence.

In the next section, first the methodology is explained, which is used to assess the relative importance of each physical process that is involved in the evolution of stratocumulus-topped boundary layers. In Sect. 3 the details of the LESs that have been performed are described. The LWP tendency during the ASTEX transition is analyzed in Sect. 4, while several sensitivity studies are discussed in Sect. 5. In the final section, a short summary of the conclusions is presented.

2 Methodology

2.1 Contributions to the LWP tendency

The cloud albedo increases for larger values of the LWP, which is defined as

$$\mathrm{LWP} = \int_{z=0}^{\infty} \rho q_\mathrm{l} \mathrm{d}z, \tag{2}$$

where q_l is the liquid water specific humidity, which is the sum of the cloud water q_c and rain water specific humidity q_r. Furthermore, ρ is the density of air and z is height. Van der Dussen et al. (2014) extended the LWP budget analysis of Randall et al. (1984) by including the contribution of cloud-base turbulent fluxes, radiation and drizzle, in

ACPD
15, 17229–17250, 2015

addition to entrainment. The resulting LWP budget equation allows for the evaluation of the relative contribution of individual physical processes to the LWP tendency, so

$$\frac{\partial \mathrm{LWP}}{\partial t} = \mathrm{Ent} + \mathrm{Base} + \mathrm{Rad} + \mathrm{Prec} + \mathrm{Subs}. \quad (3)$$

Here, the abbreviations indicate LWP tendencies as a result of entrainment of free tropospheric air into the boundary layer at the top of the stratocumulus layer (Ent), turbulent fluxes of total specific humidity q_t and liquid water potential temperature θ_l at the base of the stratocumulus layer (Base), divergence of the net radiative flux over the stratocumulus layer (Rad), divergence of the precipitation flux over the stratocumulus layer (Prec) and large-scale subsidence (Subs). We refer to Van der Dussen et al. (2014) for a derivation of these terms. Below, the results are repeated for convenience.

The LWP tendency due to large-scale subsidence can be written as:

$$\mathrm{Subs} = -\rho h \Gamma_{q_l} \overline{w}(z_i), \quad (4)$$

in which h is the thickness of the stratocumulus cloud layer, $\overline{w}$ is the large-scale vertical velocity and $\Gamma_{q_l} = -\partial q_l / \partial z < 0$ is the lapse rate of q_l. The value of Γ_{q_l} is approximated by assuming a moist adiabatic temperature lapse rate. Subsidence acts to decrease the LWP by pushing the stratocumulus cloud top down.

Note that all variables used in the current study are slab-averages unless specifically stated otherwise. The overbar that is commonly used to indicate a slab-averaged variable is omitted for notational convenience, except for the turbulent fluxes and variances.

The entrainment contribution to the LWP tendency is as follows:

$$\mathrm{Ent} = \rho w_e \left(\eta \Delta q_t - \Pi \gamma \eta \Delta \theta_l - h \Gamma_{q_l} \right), \quad (5)$$

where Δq_t and $\Delta \theta_l$ indicate the inversion jumps of q_t and θ_l respectively, Π is the Exner function and $\gamma = \partial q_s / \partial T \approx 0.55\,\mathrm{g\,kg^{-1}\,K^{-1}}$ is described by the Clausius–Clapeyron

ACPD
15, 17229–17250, 2015

cc BY

relation. Furthermore, η is a thermodynamic factor that depends mainly on temperature and is given by

$$\eta = \left(1 + \frac{L_\mathrm{v}\gamma}{c_p}\right)^{-1} \approx 0.4,$$

with c_p the specific heat of air at constant pressure and L_v the latent heat of vaporization.

The remaining three terms of Eq. (3) are

$$\mathrm{Base} = \rho\eta\left[\overline{w'q_\mathrm{t}'}(z_\mathrm{b}) - \Pi\gamma\overline{w'\theta_\mathrm{l}'}(z_\mathrm{b})\right], \tag{6}$$

$$\mathrm{Rad} = \frac{\eta\gamma}{c_p}\left[F_\mathrm{rad}(z_\mathrm{t}) - F_\mathrm{rad}(z_\mathrm{b})\right], \tag{7}$$

$$\mathrm{Prec} = -\rho\left[P(z_\mathrm{t}) - P(z_\mathrm{b})\right]. \tag{8}$$

Here, $\overline{w'q_\mathrm{t}'}$ and $\overline{w'\theta_\mathrm{l}'}$ are the turbulent fluxes of q_t and θ_l. Furthermore, z_b and z_t are stratocumulus base and top height, respectively, F_rad is the radiation flux in W m^{-2} and P is the precipitation flux in m s^{-1}, both of which are defined negative downward.

2.2 Evaluation of cloud boundaries

The LWP budget equation described in the previous section is used to quantify the relative importance of the individual physical processes to the total LWP tendency. To this end, Eqs. (4)–8) will be evaluated using slab-averaged vertical profiles derived from the LES. To accurately evaluate the LWP tendencies with this method, it is important to properly define the top and bottom interfaces of the stratocumulus layer.

The stratocumulus base height is defined as the minimum height where the slab-averaged cloud fraction σ exceeds 0.4,

$$z_\mathrm{b} = \min(z), \quad \text{where } \sigma(z) > 0.4. \tag{9}$$

Discussion Paper | Discussion Paper | Discussion Paper | Discussion Paper |

ACPD
15, 17229–17250, 2015

How large-scale subsidence affects stratocumulus transitions

van der Dussen et al.

Title Page
Abstract | Introduction
Conclusions | References
Tables | Figures
◀◀ | ▶▶
◀ | ▶
Back | Close
Full Screen / Esc
Printer-friendly Version
Interactive Discussion

CC BY

The criterion is chosen such that the cumulus clouds below the stratocumulus layer are ignored. The analysis is quite insensitive to the critical σ value as stratocumulus base height is typically well defined in terms of the cloud fraction profile. Any value between $\sigma \approx 0.2$ and 0.8 can be used.

Some more care is required for the definition of stratocumulus top height z_t. To take into account the vertical undulations in the cloud top and in particular its effect on the horizontal slab mean flux profiles (van Zanten et al., 1999), the budget analysis is performed up to the top of the inversion layer, the height of which is defined as z_i^+. Hence, in Eq. (7)

$$z_t = z_i^+. \quad (10)$$

There is practically no cloud water at this level, so that the precipitation flux is negligible, $P(z_t) \approx 0$.

The upper and lower boundaries of the inversion layer are determined on the basis of the profile of the variance of θ_l as follows (Yamaguchi et al., 2011):

$$z_i^+ = z, \quad \text{where } \overline{\theta_l'^2} = 0.05 \cdot \max\left(\overline{\theta_l'^2}\right) \text{ and } z > z_{max}, \quad (11a)$$

$$z_i^- = z, \quad \text{where } \overline{\theta_l'^2} = 0.05 \cdot \max\left(\overline{\theta_l'^2}\right) \text{ and } z < z_{max}. \quad (11b)$$

Here, z_{max} is the height at which the maximum of the $\overline{\theta_l'^2}$ profile is located. Linear interpolation is used between the grid levels to determine z_i^+ and z_i^-. The peak of the slab-averaged $\overline{\theta_l'^2}$ profile is very well defined, such that the values of z_i^+ and z_i^- do not dependent strongly on the rather arbitrary criteria in Eq. (11).

The inversion jump of a conserved variable φ is defined as the difference between the variable at the top and at the base of the inversion layer

$$\Delta\varphi = \varphi(z_i^+) - \varphi(z_i^-). \quad (12)$$

ACPD
15, 17229–17250, 2015

CC BY

3 Setup

3.1 Forcings and domain

In Sect. 4 the LWP budget of the Atlantic Stratocumulus Transition EXperiment (ASTEX, Albrecht et al., 1995) case is analyzed, for which the initial conditions and forcings were described by Van der Dussen et al. (2013). The simulation lasts 40 h and features diurnally varying insolation. During the transition, the boundary layer evolves from relatively shallow and well mixed to deep and decoupled with cumulus updrafts underneath a thin broken stratocumulus layer. The results of this case are used here to illustrate how the methodology described in the previous section can help to understand the often complex interaction between processes that together determine the evolution of the stratocumulus layer.

Many of the forcings and boundary conditions for the ASTEX case, such as the subsidence velocity, the solar zenith angle and the geostrophic wind velocities, vary with time. This could make the interpretation of sensitivity experiments unnecessarily complicated. The forcings of the ASTEX case have therefore been idealized for the sensitivity experiments, as follows.

A diurnally averaged solar zenith angle of 68.72° is prescribed, resulting in a constant downwelling shortwave radiative flux of approximately 494 $\mathrm{W\,m^{-2}}$ at the top of the atmosphere. Furthermore, the geostrophic wind velocities are kept constant and equal to the initial horizontal velocities, which are constant with height at $(u, v) = (5.5, 0)\,\mathrm{m\,s^{-1}}$. Hence, the mean wind speed is approximately constant in time. The microphysics parameterization scheme is disabled.

For the sensitivity simulations, the prescribed large-scale subsidence profile is kept constant with time. It is defined as:

$$\overline{w}(z) = \begin{cases} -Dz & \text{for} \quad z \leq z_D \\ -Dz_D & \text{otherwise,} \end{cases}$$

ACPD
15, 17229–17250, 2015

How large-scale subsidence affects stratocumulus transitions

van der Dussen et al.

cc BY

where z_D = 500 m and D is the large-scale divergence of horizontal winds. The only boundary condition that varies in time is the SST, which increases linearly from 291 to 297 K over the course of the 60 h simulations.

The horizontal domain size is 4800 m × 4800 m, divided into 192 × 192 gridpoints that are spaced 25 m apart. In the vertical direction, the resolution is varied from 10 m at the surface to 5 m for z between 500 and 2300 m. Above, the vertical grid spacing is increased by 5 % per level up to a height of 3 km, resulting in a total of 500 levels.

3.2 Model details

The Dutch Atmospheric LES (DALES) model version 4.0 was used to perform the simulations. Compared to version 3.2 that was described by Heus et al. (2010), this version has an anelastic core (Böing et al., 2012). The model settings and parameterization schemes that were used are identical to those described by Van der Dussen et al. (2015).

4 ASTEX transition

The LWP for the ASTEX case is shown in Fig. 1a as a function of time. The LWP evolution is qualitatively similar to that obtained with DALES version 3.2 (Van der Dussen et al., 2013), despite the fact that different radiation and microphysics parameterization schemes are used in the present study.

The tendency of the LWP is indicated by the thick black line in Fig. 1b. The thin black line in this figure shows the net LWP tendency diagnosed using Eq. (3), which agrees very well with the actual LWP tendency.

Interestingly, the net LWP tendency is small as compared to the contributions from entrainment, radiation and turbulent fluxes at stratocumulus base height. The simulation starts approximately at midnight. During the initial 8 h, the contribution of the

ACPD
15, 17229–17250, 2015

cc BY

radiation to the LWP tendency is therefore solely due to longwave radiative cooling. This contribution is large and causes the stratocumulus layer to thicken.

The increase of the LWP triggers additional precipitation, so that its thinning contribution increases until it approximately balances the radiative tendency and the net LWP tendency decreases.

After about 8 h of simulation, the sun rises. The stratocumulus layer absorbs the solar radiation, which causes a warming that partly offsets the longwave radiative cooling so that the net thickening effect due to radiation diminishes during the day. The thinner stratocumulus layer supports only little precipitation, such that the thinning tendency due to precipitation reduces to approximately zero. The feedback of the LWP on the generation of precipitation acts as a buffering mechanism, leveling out variations of the LWP on timescales of several hours.

The decrease of the net radiative cooling during the day also diminishes the production of turbulence in the cloud layer, which is reflected by the decrease of the magnitudes of the contributions of the entrainment and of the turbulent fluxes at stratocumulus base. Interestingly, the response of the turbulence intensity to the change of the radiative forcing seems to be delayed somewhat, causing the minimum LWP in Fig. 1a to occur about two to four hours after midday.

The contribution of the large-scale subsidence to the LWP is relatively small and negative. Its thinning effect decreases as the stratocumulus cloud thins, which is due to the h dependence in Eq. (4).

During the second night, after about 20 h, the thinning due to entrainment is approximately balanced by equal thickening contributions by the radiative cooling and the fluxes at cloud base. Surprisingly, the contributions due to subsidence and precipitation are negligible at this stage. As a result the LWP decreases only very slightly until the cloud layer starts to break up at the beginning of the second day.

ACPD
15, 17229–17250, 2015

5 Sensitivity to the large-scale subsidence

5.1 Effect on cloud properties

The projected cloud cover σ is shown in Fig. 2a for the three sensitivity simulations in which the large-scale subsidence velocity is varied. The results demonstrate clearly that a weakening of the large-scale subsidence extends the lifetime of the stratocumulus layer, thereby corroborating the findings of Svensson et al. (2000) and Sandu and Stevens (2011). Figure 2b furthermore shows that a weakening of the subsidence causes the LWP to increase. The large differences among the simulations are somewhat surprising, as it was shown in the previous that the contribution of subsidence to the LWP tendency is relatively small.

Despite the absence of precipitation and a diurnal cycle, the transitions with the idealized forcings are qualitatively similar to the original ASTEX transition (Fig. 1a). However, the stratocumulus breakup occurs later in the sensitivity experiments. In the second half of the original ASTEX transition, the magnitude of the horizontal wind velocity decreases, which drastically reduces the surface humidity flux and likely causes the transition to accelerate (Van der Dussen et al., 2013). In the sensitivity experiments, on the other hand, the horizontal wind speed is constant in time so that the stratocumulus layer is maintained longer at the end of the transition.

Figure 3a shows the top and base interfaces of the stratocumulus layer as defined in Sect. 2.2. Differences in stratocumulus top height start to occur soon after the start of the simulations. Stratocumulus base height, on the other hand, remains unaffected for roughly 15 h. This suggests that the difference in the subsidence velocity does not strongly affect the temperature and humidity profiles in the bulk of the boundary layer during this period. Later on in the simulations, differences in the stratocumulus base height also start occurring.

It is interesting to note that the differences of the inversion height among the simulations are roughly a factor of two larger than would be expected on the basis of the difference in the subsidence rate alone. As can be seen in Fig. 3b, the entrainment rate is found to increase as subsidence weakens. Such an increase was also found by Sandu and Stevens (2011) and it is most likely the result of the larger stratocumulus thickness h, which typically causes the cloud layer to be more energetic eventually leading to enhanced entrainment (e.g. Nicholls and Turton, 1986; Jones et al., 2014).

5.2 Analysis of LWP budget

To determine how much each of the physical processes that affect the LWP contribute to the LWP differences among the simulations, the terms of the LWP budget equation are shown individually in the left column of Fig. 4. Note that the scale of the vertical axis of the subfigures varies significantly.

Figure 4a shows the LWP tendency due to subsidence. Evidently, the cloud thinning due to subsidence is less strong for the weaker subsidence cases. The difference among the simulations is about $3\,\mathrm{g\,m^{-2}\,h^{-1}}$ during the first part of the transition and slowly decreases with time. For the LWP tendencies due to radiation, entrainment and cloud base turbulent fluxes, shown in Fig. 4c, e and g respectively, the data do not show a clear trend due to the significant amount of noise.

In order to obtain a clearer picture of how large the LWP differences caused by each of the individual processes are, the following steps are taken. First, the $-Dz_D = -4.5\,\mathrm{mm\,s^{-1}}$ simulation indicated by the black lines in Figs. 2 and 3 is chosen as a reference. Then, the differences with respect to this reference of the LWP tendency due to each process is determined. These differences are integrated in time to give the LWP difference among the simulations that is solely due to that process. So, for the subsidence term

$$\delta\mathrm{LWP}|_{\mathrm{Subs}}(t) = \int_0^t \delta\mathrm{Subs}(t')\mathrm{d}t' = \int_0^t \mathrm{Subs}(t') - \mathrm{Subs}^{\mathrm{r}}(t')\mathrm{d}t', \qquad (13)$$

where δ denotes the difference of a variable with respect to the reference simulation that is denoted by a superscripted “r”. Similarly, the LWP differences solely due to the

ACPD
15, 17229–17250, 2015

CC BY

Rad, Ent and Base terms in Eqs. (5) to (7) were calculated. The results are shown for each of the processes by the plots in the right hand column of Fig. 4.

The LWP difference caused solely by subsidence is shown in Fig. 4b. Consider the simulation indicated by the blue line, which has a weaker subsidence as compared to the reference simulation. The smaller cloud thinning tendency due to subsidence for this case causes a positive contribution to the LWP difference, δLWP, that increases approximately linearly with time up to a value of about $100\,\mathrm{g\,m^{-2}}$.

The absorption of shortwave radiation by a stratocumulus layer increases with the LWP (Van der Dussen et al., 2013). So, as subsidence is weakened and the LWP increases, the absorption of shortwave radiation also increases. The net cloud thickening effect due to radiative cooling is therefore reduced. Hence, the LWP difference with the reference is negative for the weak subsidence simulation (Fig. 4d) and compensates for much of the LWP difference due to subsidence in the second part of the transition.

The LWP difference as a results of entrainment is less straightforward to understand. In the previous section, it was shown that the entrainment rate is largest for the weakest subsidence simulation. As entrainment causes drying and warming of the stratocumulus layer, this higher entrainment velocity is expected to cause a negative contribution to δLWP. However, Fig. 4f shows that it is the other way around: for the lowest subsidence case with the highest entrainment rate, the contribution of entrainment to δLWP is positive. This has two main causes. First, the magnitude of the inversion jump of humidity Δq_t decreases as subsidence is weakened. This decrease exceeds $0.5\,\mathrm{g\,kg^{-1}}$ or 10 % at the end of the simulations and weakens the drying of the stratocumulus layer due to entrainment. Second, the equation for the contribution of entrainment to the LWP tendency in Eq. (5) consists of three terms. The last of these terms accounts for the deepening of the cloud layer due to entrainment. This term increases with the cloud thickness h. For the weak subsidence simulation, h is greater than for the reference simulation. Together with the smaller Δq_t, this causes the cloud thinning tendency due to entrainment to be less strong for the weak subsidence case, despite the higher entrainment rate.

ACPD
15, 17229–17250, 2015

CC BY

Figure 4h shows the contribution of cloud base turbulent fluxes to δLWP. The boundary layer is deepest for the weak subsidence simulation, which causes a slight reduction of the turbulent transport of humidity to the cloud layer. Hence, the contribution of the cloud base fluxes to δLWP is on average negative for the weak subsidence simulation indicated by the blue line.

From the comparison of Fig. 4f and h it is clear that the cloud base turbulent flux contribution to δLWP is strongly anticorrelated with that of entrainment. The sum of both contributions is therefore almost zero. In other words, the net effect of these turbulent fluxes to the LWP difference among the cases is very small. The LWP differences in Fig. 2b are therefore mainly due to the direct effect of large-scale subsidence on the LWP tendency and the subsequent change of the absorption of shortwave radiation.

6 Conclusions

Several studies have shown that as a result of warming of the climate the Hadley circulation might weaken, leading to a weakening of the large-scale subsidence in the subtropical stratocumulus areas. Several modeling studies (Svensson et al., 2000; Sandu and Stevens, 2011) and recent observational evidence (Myers and Norris, 2013) suggest that such a decrease can lead to thicker and more persistent stratocumulus clouds.

To investigate how the large-scale subsidence affects stratocumulus layers, a method is applied in the current study to analyze the individual contributions of five different physical processes to the LWP tendency of an adiabatic stratocumulus layer. As an illustration of the use of this method, it was first applied to LES results of the ASTEX stratocumulus transition (Van der Dussen et al., 2013). The results show among others that subsidence tends to reduce the LWP by pushing down the cloud top. Longwave radiative cooling tends to increase the LWP, while the absorption of shortwave radiation during the day diminishes the net radiative effect. Entrainment dries and warms the cloud layer resulting in a strong cloud thinning effect that increases as the transition progresses. The transport of humidity toward the cloud layer by turbulent fluxes counteracts this drying, causing a significant positive effect on the LWP tendency. The results furthermore indicate that the cloud thinning contribution of the large-scale subsidence is small as compared to the other contributions.

Despite this relatively small contribution to the LWP tendency, more idealized sensitivity simulations show that decreasing the subsidence velocity extends the lifetime of the stratocumulus layer. Moreover, it causes the LWP to be significantly higher throughout the entire transition. The thicker stratocumulus layer in the weak subsidence cases tends to absorb more solar radiation, which partly offsets the LWP difference due to subsidence in the second part of the simulations.

It was shown that a weakening of the large-scale subsidence causes enhanced entrainment that amplifies the differences of the inversion height among the simulations. Counterintuitively, this higher entrainment rate does not result in a stronger cloud thinning tendency with respect to the reference simulation, which is likely due to a reduction of the magnitude of the inversion jumps of q_t and θ_l and the greater cloud thickness.

The cloud thickening contribution of the cloud base turbulent fluxes decreases somewhat for the weaker subsidence cases as a result of the greater boundary layer depth. This decrease is strongly anticorrelated to the LWP increase as a result of entrainment, such that the total contribution of the turbulent fluxes to the LWP difference among the cases is negligible.

The results of the current study suggest that it is likely that a weakening of the large-scale subsidence in the subtropics due to the weakening of the Hadley circulation in a future climate increases the average LWP as well as the occurrence of subtropical stratocumulus clouds.

Acknowledgements. The investigations were done as part of the European Union CLoud Intercomparison, Process Study and Evaluation (EUCLIPSE) project, funded under Framework Program 7 of the European Union. The work was sponsored by the National Computing Facilities Foundation (NCF) for the use of supercomputer facilities.

ACPD
15, 17229–17250, 2015

Discussion Paper | Discussion Paper | Discussion Paper | Discussion Paper |

References

Albrecht, B. A., Bretherton, C. S., Johnson, D., Scubert, W. H., and Frisch, A. S.: The Atlantic Stratocumulus Transition Experiment–ASTEX, B. Am. Meteorol. Soc., 76, 889–904, doi:10.1175/1520-0477%281995%29076%3C0889%3ATASTE%3E2.0.CO%3B2, 1995. 17236

Blossey, P. N., Bretherton, C. S., Zhang, M., Cheng, A., Endo, S., Heus, T., Liu, Y., Lock, A. P., de Roode, S. R., and Xu, K.-M.: Marine low cloud sensitivity to an idealized climate change: the CGILS LES intercomparison, J. Adv. Model. Earth Syst., 5, 234–258, doi:10.1002/jame.20025, 2013. 17231

Böing, S. J., Jonker, H. J. J., Siebesma, A. P., and Grabowski, W. W.: Influence of the subcloud layer on the development of a deep convective ensemble, J. Atmos. Sci., 69, 2682–2698, doi:10.1175/JAS-D-11-0317.1, 2012. 17237

Bretherton, C. S. and Blossey, P. N.: Low cloud reduction in a greenhouse-warmed climate: results from Lagrangian LES of a subtropical marine cloudiness transition, J. Adv. Model. Earth Syst., 6, 91–114, doi:10.1002/2013MS000250, 2014. 17231

Bretherton, C. S., Austin, P., and Siems, S. T.: Cloudiness and marine boundary layer dynamics in the ASTEX Lagrangian experiments. Part II: Cloudiness, drizzle, surface fluxes, and entrainment, J. Atmos. Sci., 52, 2724–2735, doi:10.1175/1520-0469%281995%29052%3C2724%3ACAMBLD%3E2.0.CO%3B2, 1995. 17232

Bretherton, C. S., Krueger, S. K., Wyant, M. C., Bechtold, P., Van Meijgaard, E., Stevens, B., and Teixeira, J.: A GCSS boundary-layer cloud model intercomparison study of the first ASTEX Lagrangian experiment, Bound.-Lay. Meteorol., 93, 341–380, doi:10.1023/A:1002005429969, 1999. 17231

Bretherton, C. S., Blossey, P. N., and Jones, C. R.: Mechanisms of marine low cloud sensitivity to idealized climate perturbations: a single-LES exploration extending the CGILS cases, J. Adv. Model. Earth Syst., 5, 316–337, doi:10.1002/jame.20019, 2013. 17231

Carman, J. K., Rossiter, D. L., Khelif, D., Jonsson, H. H., Faloona, I. C., and Chuang, P. Y.: Observational constraints on entrainment and the entrainment interface layer in stratocumulus, Atmos. Chem. Phys., 12, 11135–11152, doi:10.5194/acp-12-11135-2012, 2012. 17232

Ciesielski, P. E., Schubert, W. H., and Johnson, R. H.: Diurnal variability of the marine boundary layer during ASTEX, J. Atmos. Sci., 58, 2355–2376, doi:10.1175/1520-0469%282001%29058%3C2355%3ADVOTMB%3E2.0.CO%3B2, 2001. 17232

CC BY

De Roode, S. R. and Duynkerke, P. G.: Observed lagrangian transition of stratocumulus into cumulus during ASTEX: mean state and turbulence structure, J. Atmos. Sci., 54, 2157–2173, doi:10.1175/1520-0469%281997%29054%3C2157%3AOLTOSI%3E2.0.CO%3B2, 1997. 17232

Duynkerke, P. G., Jonker, P. J., Chlond, A., Van Zanten, M. C., Cuxart, J., Clark, P., Sanchez, E., Martin, G., Lenderink, G., and Teixeira, J.: Intercomparison of three- and one-dimensional model simulations and aircraft observations of stratocumulus, Bound.-Lay. Meteorol., 92, 453–487, doi:10.1023/A:1002006919256, 1999. 17232

Held, I. M. and Soden, B. J.: Robust responses of the hydrological cycle to global warming, J. Climate, 19, 5686–5699, doi:10.1175/JCLI3990.1, 2006. 17230

Heus, T., van Heerwaarden, C. C., Jonker, H. J. J., Pier Siebesma, A., Axelsen, S., van den Dries, K., Geoffroy, O., Moene, A. F., Pino, D., de Roode, S. R., and Vilà-Guerau de Arellano, J.: Formulation of the Dutch Atmospheric Large-Eddy Simulation (DALES) and overview of its applications, Geosci. Model Dev., 3, 415–444, doi:10.5194/gmd-3-415-2010, 2010. 17237

Jones, C. R., Bretherton, C. S., and Blossey, P. N.: Fast stratocumulus time scale in mixed layer model and large eddy simulation, J. Adv. Model. Earth Syst., 6, 206–222, doi:10.1002/2013MS000289, 2014. 17240

Myers, T. A. and Norris, J. R.: Observational evidence that enhanced subsidence reduces subtropical marine boundary layer cloudiness, J. Climate, 26, 7507–7524, doi:10.1175/JCLI-D-12-00736.1, 2013. 17231, 17242

Nicholls, S. and Turton, J. D.: An observational study of the structure of stratiform cloud sheets: Part II. Entrainment, Q. J. Roy. Meteor. Soc., 112, 461–480, doi:10.1002/qj.49711247210, 1986. 17240

Park, S., Leovy, C. B., and Rozendaal, M. A.: A new heuristic Lagrangian marine boundary layer cloud model, J. Atmos. Sci., 61, 3002–3024, doi:10.1175/JAS-3344.1, 2004. 17231

Randall, D. A., Coakley, J. A., Lenschow, D. H., Fairall, C. W., and Kropfli, R. A.: Outlook for research on subtropical marine stratification clouds, B. Am. Meteorol. Soc., 65, 1290–1301, doi:10.1175/1520-0477%281984%29065%3C1290%3AOFROSM%3E2.0.CO%3B2, 1984. 17232

Sandu, I. and Stevens, B.: On the factors modulating the stratocumulus to cumulus transitions, J. Atmos. Sci., 68, 1865–1881, doi:10.1175/2011JAS3614.1, 2011. 17231, 17239, 17240, 17242

ACPD
15, 17229–17250, 2015

How large-scale subsidence affects stratocumulus transitions

van der Dussen et al.

CC BY

Svensson, G., Tjernström, M., and Koračin, D.: The sensitivity of a stratocumulus transition: model simulations of the ASTEX first Lagrangian, Bound.-Lay. Meteorol., 95, 57–90, doi:10.1023/A:1002434314651, 2000. 17231, 17239, 17242

Van der Dussen, J. J., de Roode, S. R., Ackerman, A. S., Blossey, P. N., Bretherton, C. S., Kurowski, M. J., Lock, A. P., Neggers, R. A. J., Sandu, I., and Siebesma, A. P.: The GASS/EUCLIPSE model intercomparison of the stratocumulus transition as observed during ASTEX: LES results, J. Adv. Model. Earth Syst., 5, 483–499, doi:10.1002/jame.20033, 2013. 17236, 17237, 17239, 17241, 17242

Van der Dussen, J. J., de Roode, S. R., and Siebesma, A. P.: Factors controlling rapid stratocumulus cloud thinning, J. Atmos. Sci., 71, 655–664, doi:10.1175/JAS-D-13-0114.1, 2014. 17232, 17233

Van der Dussen, J. J., de Roode, S. R., Gesso, S. D., and Siebesma, A. P.: An LES model study of the influence of the free tropospheric thermodynamic conditions on the stratocumulus response to a climate perturbation, J. Adv. Model. Earth Syst., 7, published online, doi:10.1002/2014MS000380, 2015. 17237

van Zanten, M. C., Duynkerke, P. G., and Cuijpers, J. W. M.: Entrainment parameterization in convective boundary layers, J. Atmos. Sci., 56, 813–828, doi:10.1175/1520-0469(1999)056<0813:EPICBL>2.0.CO;2, 1999. 17235

Vecchi, G. A. and Soden, B. J.: Global warming and the weakening of the tropical circulation, J. Climate, 20, 4316–4340, doi:10.1175/JCLI4258.1, 2007. 17230

Wood, R. and Bretherton, C. S.: Boundary layer depth, entrainment, and decoupling in the cloud-capped subtropical and tropical marine boundary layer, J. Climate, 17, 3576–3588, doi:10.1175/1520-0442%282004%29017%3C3576%3ABLDEAD%3E2.0.CO%3B2, 2004. 17231

Wyant, M. C., Bretherton, C. S., Rand, H. A., and Stevens, D. E.: Numerical simulations and a conceptual model of the stratocumulus to trade cumulus transition, J. Atmos. Sci., 54, 168–192, doi:10.1175/1520-0469(1997)054<0168:NSAACM>2.0.CO;2, 1997. 17231

Yamaguchi, T., Randall, D. A., and Khairoutdinov, M. F.: Cloud modeling tests of the ULTIMATE-MACHO scalar advection scheme, Mon. Weather Rev., 139, 3248–3264, doi:10.1175/MWR-D-10-05044.1, 2011. 17235

ACPD
15, 17229–17250, 2015

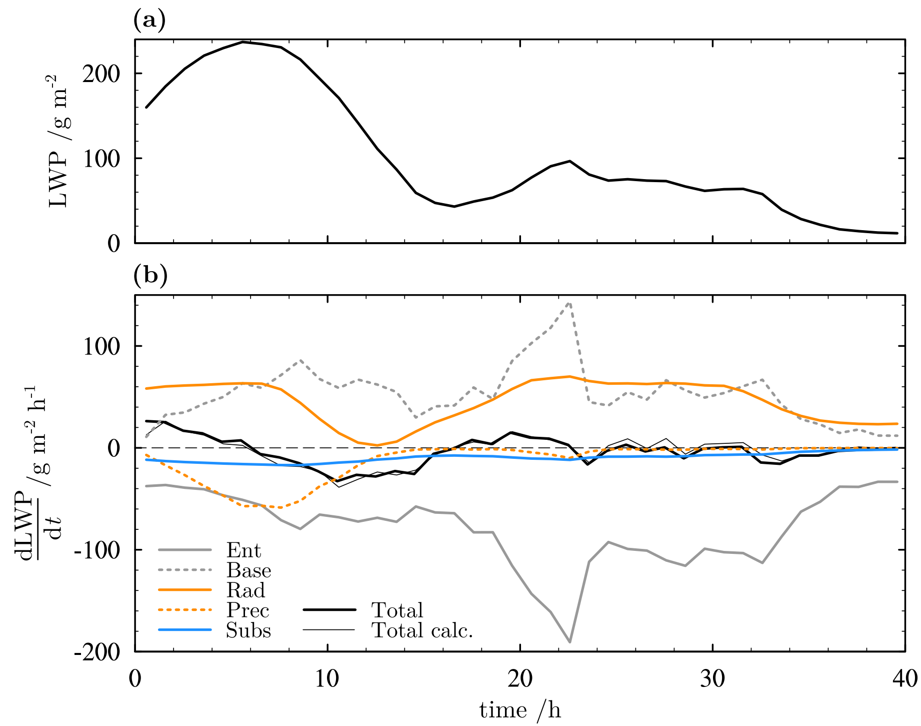

Figure 1. (a) The LWP as function of time for the ASTEX transition simulation. **(b)** The tendency of the LWP as a function of time, split into the contributions from the individual physical processes according to Eq. (3). Line colors and styles as denoted by the legend. The horizontal dashed black line indicates the zero tendency level as a reference.

ACPD
15, 17229–17250, 2015

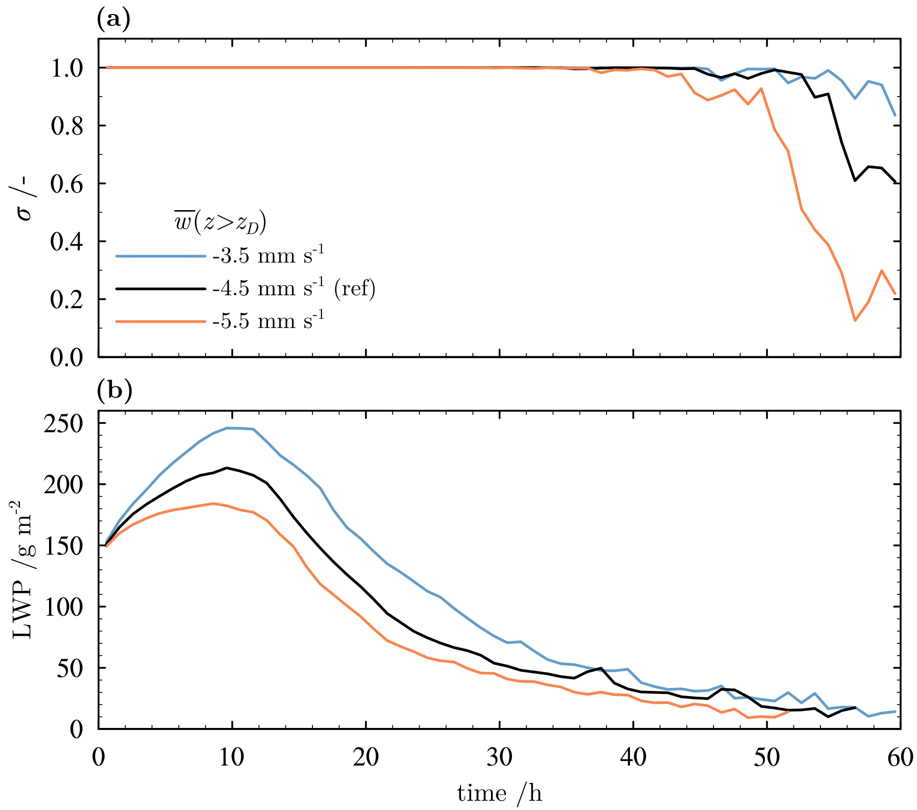

Figure 2. (a) The projected cloud cover σ and **(b)** the LWP as a function of time for the the sensitivity simulations in which the large-scale subsidence velocity is varied as indicated by the legend.

ACPD
15, 17229–17250, 2015

How large-scale subsidence affects stratocumulus transitions

van der Dussen et al.

Title Page
Abstract | Introduction
Conclusions | References
Tables | Figures
◀| |▶
◀ ▶
Back | Close
Full Screen / Esc
Printer-friendly Version
Interactive Discussion

cc BY

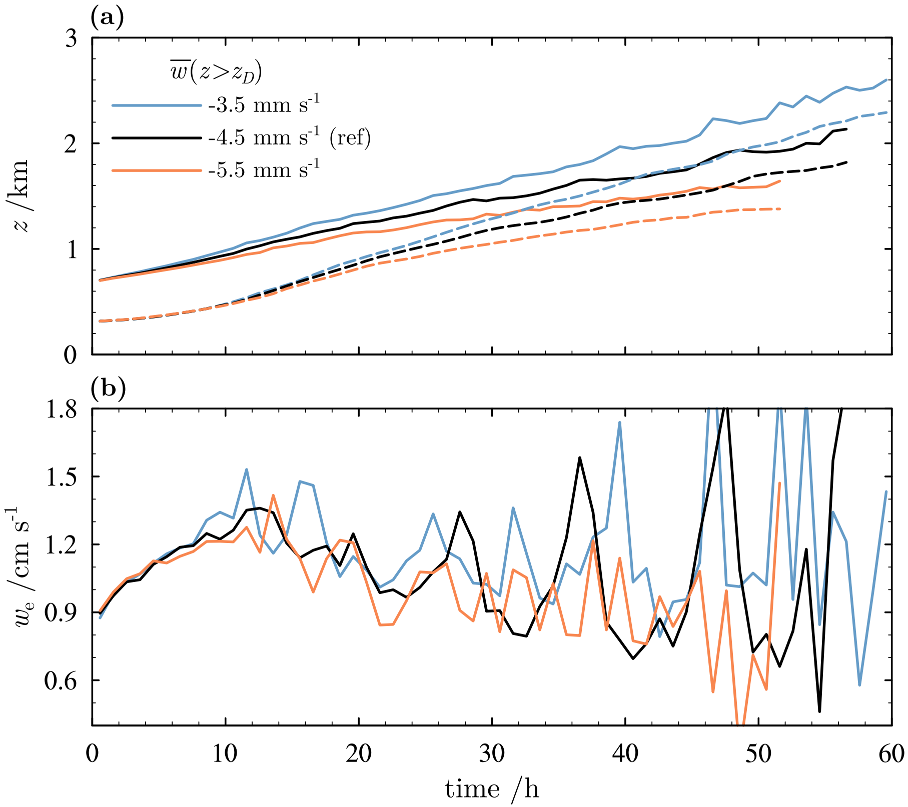

Figure 3. (a) The stratocumulus top (solid) and base height (dashed) and **(b)** the entrainment velocity as a function of time for the subsidence sensitivity simulations.

ACPD
15, 17229–17250, 2015

How large-scale subsidence affects stratocumulus transitions

van der Dussen et al.

Title Page
Abstract Introduction
Conclusions References
Tables Figures
◀ ▶
Back Close
Full Screen / Esc
Printer-friendly Version
Interactive Discussion

CC BY

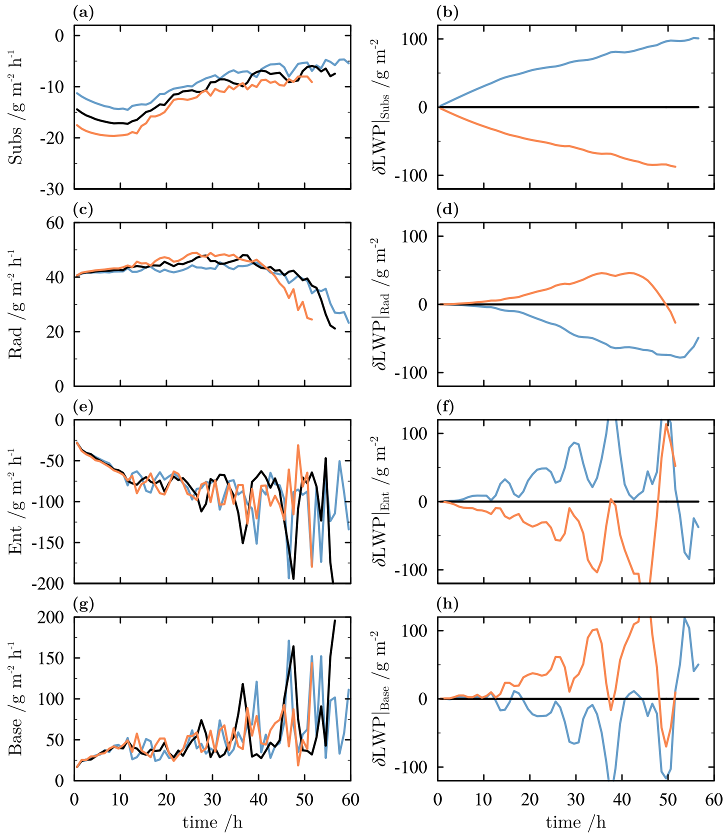

Figure 4. The LWP tendencies due to **(a)** subsidence, **(c)** radiation, **(e)** entrainment and **(g)** cloud base turbulent fluxes as a function of time for each of the sensitivity simulations. The LWP differences with the reference (black) due to each of these processes have been calculated according to Eq. (13) and are shown in panels **(b)**, **(d)**, **(f)**, and **(h)**, respectively. Colors according to the legend in Fig. 3a.